On the statistical nature of distinct cycles in global warming variables

Knut Lehre Seip and Øyvind Grøn

Oslo and Akershus university college for applied sciences

Faculty of technology, art and design

Pilestredet 35, Oslo, NORWAY

Knut.lehre.seip@hioa.no

3700 words

Oceanic time series, Southern oscillation index, Pacific decadal oscillation, interactions, leading-lagging relations, internal dynamics

Abstract

Cycle times found in many oceanic time series have been explained with references to external mechanisms that act on the systems. Here we show that when we extract cycle times from 100 sets of paired random series, we find six distinct clusters of common cycle times ranging from about 3 years to about 32 years. Cycle times, CT, get shorter when one series in a pair is an increasingly stronger leading series, measured as LL-strength, to the other, CT ≈ - (minus) LL-strength. This may explain the frequent finding that many global warming time series, e.g., the Southern oscillation index and the Pacific decadal oscillation, show distinct cycle times (Power spectral analysis: 3-5, 7-8, 13-15, 22-24, and 29-30 years). An important implication of these findings is that processes that strengthen the impact of one ocean variable on another may cause more frequent adverse climate conditions.

1. INTRODUCTION

Cycle times for global warming series, like global sea surface temperatures and ocean currents are studied extensively, and several attempts have been made to associate the cycles with external and internal driving forces. Recently, the term El Niño- Southern oscillation, ENSO, diversity has been used to characterize the many cycle times found in the ENSO time series (Capotondi et al. 2015). Six possible interactions have been suggested to explain cycles and phase shifts mechanistically: i) *external factors*; Keeling and Whorf (1997), Munk et al. (2002) and Ray (2007) discuss connections between climate variability and tidal cycles. Meehl et al. (2009) and Andrews et al. (2015) examine possible effects of total solar irradiance on the Pacific and the North Atlantic oscillation, respectively. Meehl et al. (2013) also include internal mechanisms by suggesting that the interdecadal Pacific oscillation, IPO, shows "transitions on its own". Cai et al. (2015) suggest in a modeling study that global warming increases the frequency of extreme La Niña events. ii) *Interaction between the ocean and the atmosphere*, atmospheric "bridges". Ray (2007) summarizes the effects of intrinsic modes of coupled atmosphere- ocean systems and beat frequencies. Zhu et al. (2011) discuss efforts to understand the decadal changes in ENSO and include stochastic atmospheric wind forcing, extratropical processes in the atmosphere and the ocean, and nonlinear processes in the climate system. iii) *interaction between layers in the ocean*, deep water "bridges", e.g., Timmermann et al. (1999), Amaya et al. (2015) iv) *interaction between distinct oceanic water bodies*, "regional bridges", e.g., DelSole et al. (2011) on the Atlantic and the Pacific basins ; v) *interaction between ocean currents and ocean borders*, like the South American continent. vi) *stochastic forcings* have been suggested as an element in explaining ocean current predictability, e.g., Wunsch (1999), Newman et al. (2011), Fedorov et al. (2015), and Di Lorenzo et al. (2015).

The intensity and frequency of cycles in ocean currents impact local conditions, e.g., the oceanographic properties and biology in the Puget Sound, Washington, Moore et al. (2008) and northern hard-water lakes, Finlay et al. (2015). Strong El Niño may have devastating consequences. An overview of mechanisms and effects for El Niño is given in Capotondi et al. (2015).

Canonical cycle times like 4, 7, 13, 22 and 30 years appear in the discussions referred to above. Here we show that for a pair of stochastic time series, where one series drives the other, characteristic cycles appear that correspond with those found in global warming time series. We suggest that more persistent leading – lagging, LL-relations between oceanic or atmospheric systems give shorter cycle times. Thus, explanations for cycle times less than ≈ 35 years may have two components, i) mechanisms that generate random movements and ii) mechanisms that make two separate ocean or atmospheric systems interact so that one leads the other with a certain time interval.

2. MATERIALS

In addition to using time series from random distributions, we examine the power spectral density of two Pacific Ocean time series that are often used in discussions of global warming.

The Southern oscillation index, SOI, or the El Niño Southern Oscillation, the ENSO. The Southern Oscillation Index, SOI, is a standardized index based on the observed sea level pressure differences between Tahiti and Darwin, Australia ($p_{Tahiti} - p_{Darwin}$). In general, negative values of the smoothed time series of the SOI (El Niño) correspond to warm ocean temperatures across the eastern and tropical Pacific. Typically, strong temperature anomalies happen at irregular intervals of two to seven years, (Allan and D'Arrigo (1999); Gehne et al. (2014)). Our version of the SOI index was obtained from the web site: http://www.bom.gov.au/climate/current/soihtm1.shtml. However, other versions exist and a survey is given in Capotondi et al. (2015)

The Pacific decadal oscillation, PDO, is closely related to the interdecadal Pacific oscillation, IPO, but has a more northern hemisphere focus, Trenberth (2015). PDO is a measure of monthly sea surface temperature anomalies over the North Pacific. The index is associated with regional temperature changes (Meehl et al. 2013). The data were obtained from the web site: http://www.atmos.washington.edu/~mantua/abst.PDO.html)

3. METHOD

We use two major methods in this study, a power spectral density, PSD, algorithm, and a novel method for finding running average leading – lagging relations and running average common cycle times for paired time series. The PSD analysis is made with the algorithm in the SigmaPlot © package, but most PSD algorithm could be used, (Press et al. 1986; Wunsch 2000). The leading –lagging, LL –method is implemented in Excel.

The running average leading –lagging, LL-method. The LL- method calculates leading, lagging relations, common cycle times and phase shifts between paired cyclic series. We define a measure for how frequent one series leads the other in the pair, the LL- strength. Since the aim of the present study is to identify common cycle times for pairs of stochastic series (uniform and Gaussian) that have LL- strength above certain levels, we calculate cycle times for all relevant leading –lagging, LL-strengths in 100 paired series and compare the cycles found with observed cycle times for SOI and PDO.

At the basis of the LL- method is the dual representation of paired cyclic time series, x (t) and y (t), as time representation (the x- axis represents time) and as phase plot where the paired time series are depicted on the x-axis and the y-axis on a 2D graph. If one series leads another with less than ½ a cycle time (for example by having causal effect on the other), then we will have persistent rotational direction of the series trajectories in the phase plot. Figure 1a and b give an example with x (t) = sin t and y (t) = sin (t + 0.785). The first series, x, could represent sea surface temperature, SST, normally peaking in July – August on the western hemisphere and is denoted by T in

the graph. The second series, y, could represent Sun insolation peaking in June and is denoted by CC in the graph. Since Sun insolation is associated with heat transfer to the sea surface, CC is a candidate cause for T. Thus, CC should peak before T, as it does in the figure. Real pairs of Sun insolation and SST do the same (Seip 2015).

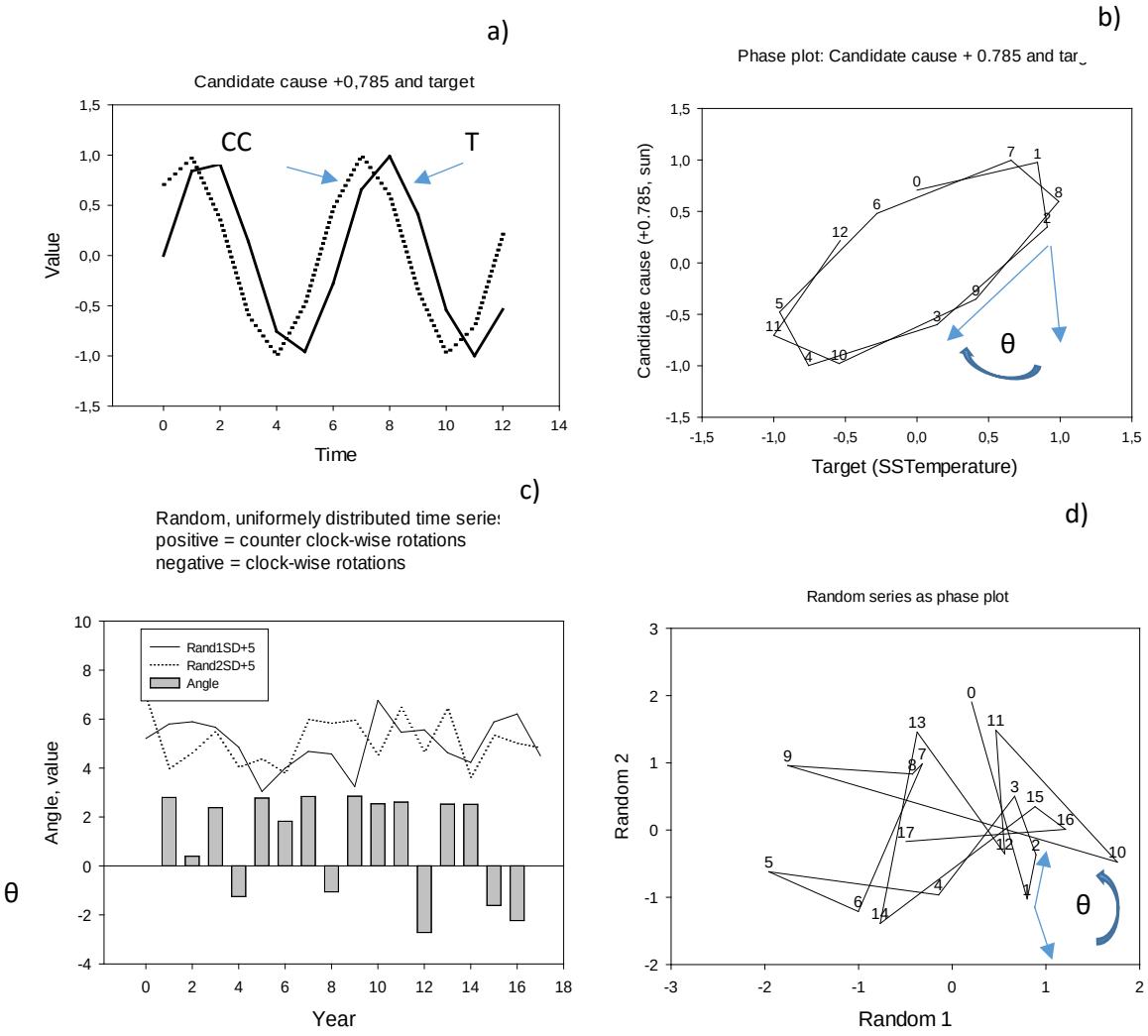

Figure 1 Time series (left) and phase plots (right). a) Two sine functions: CC is candidate cause and T is target. The candidate cause, CC, peaks before the target, T. b) In a phase plot with T on the x- axis and CC on the y-axis the time series rotates clock-wise (negative by definition), θ is the angle between two consecutive trajectories. c) Upper part: time series based on random numbers drawn from a uniform distribution; lower part: running angles. d) Phase plot for the time series in c. Points on the trajectories are numbered consecutively. Notice that the first angle 0-1-2 is positive (rotate counter clock-wise).

We explain the leading – lagging, LL method in 6 steps.

Step. 1. The random series. We made two series based on random numbers drawn

from a uniform distribution and from a pseudo normal distribution using a Box – Muller transform. The series were thereafter normalized to unit standard deviation. Figure 1c shows an example of two time series drawn from uniform random distributions and Fig 1d shows the corresponding trajectories in the phase plot.

Step 2. Rotational directions. We then calculated the angles θ between two successive trajectories $\mathbf{v}_1$ and $\mathbf{v}_2$ through 3 successive points in phase space as:[1]

$$\theta = sign(\mathbf{v}_1 \times \mathbf{v}_2) \cdot \text{Arccos}\left(\frac{\mathbf{v}_1 \cdot \mathbf{v}_2}{|\mathbf{v}_1||\mathbf{v}_2|} \right). \quad (1)$$

The rotational direction for the paired series in Figure 1c, upper part, is shown in the lower part as positive bars (counter clock-wise rotations) and negative bars (clock-wise rotations).

Step 3. The strength, LL - strength, of the mechanisms that cause two variables to either rotate clock-wise or counter clock-wise in a phase portrait is measured by the number of positive rotations, N_{pos} minus the number of negative rotations, N_{neg}, relative to the total number of rotations over a certain period, in this study, 9 and 13 years. (Common low-pass filters for global warming variables used in the literature typically is 5 years to 13 years, Chylek et al. (2014 a), McCarthy et al. (2015)).

$$(2) \qquad LL = (N_{pos} - N_{neg})/(N_{pos} + N_{neg}).$$

This means that we can assess the persistence of the rotational direction. We use the nomenclature: LL(x, y) ∈ [-1, 1] for leading- lagging strength: LL (x, y) < 0 implies that y leads x, y→x; LL(x, y) > 0 implies that x leads y, x→y. In a range around LL(x,y) = 0 no LL- relations are significant.

Significance levels were calculated with Monte Carlo simulations. We found the 95% confidence interval for the mean value (zero per definition) to be ± 0.32, that is, in a phase plot the series cycle persistently clock-wise or significantly counter clock-wise corresponding to significantly leading - lagging signatures for the series. We also calculated the number of paired time series sections with increasing LL- strength for 100 pairs of uniformly random series 130 time steps long. There is a conspicuous decline in the number of pairs that are > 4 time steps long. Supplementary material 1 shows a graph for the number of series with a certain length versus the number of persistent leading time steps.

Step 4. The cycle time, CT, of two paired series that interact, can be approximated as:

$$(3) \qquad CT = n \times 2\pi \,/\, \textstyle\sum_2^{n-1} \theta_{i-1,i,i+1}.$$

Where $\theta_{i-1,I,i+1}$ is the angle between two vectors defined by 3 consecutive points as in Eq. 1. The cycle times are first calculated for two consecutive trajectories (based on 3 time steps) and thereafter averaged over 9 or 13 consecutive time steps. The average

[1] With x- coordinates in A1 to A3 and y-coordinates in B1 to B3 the angle is calculated by pasting the following Excel expression into C2: =SIGN((A2-A1)*(B3-B2)-(B2-B1)*(A3-A2))*ACOS(((A2-A1)*(A3-A2) + (B2-B1)*(B3-B2))/(SQRT((A2-A1)^2+(B2-B1)^2)*SQRT((A3-A2)^2+(B3-B2)^2))).

of 9 and 13 time steps is a trade-off between the possibility of detecting changes in leading – lagging, LL- relations and obtaining significant LL- strength.

Step 5 Amplitude. The amplitudes were calculated as the running average difference between maximum and minimum values over increasingly longer time window approximately corresponding to the cycle times found in initial simulations.

Step 6. Monte Carlo simulations. For the illustration in Figure 1c, we used time series that were 17 time steps long, allowing the calculation of 16 rotational angles and 8 running average LL- strength measures. (Since the strength measures were averaged over 9 time steps, 4 steps in front and 4 steps at the end, this example only allows calculations of 8 running average values.)

An expanded explanation of the method is given in Seip and Grøn (2015) and transitions between normal and uniform distributions in the appendix to Seip et al. (1990).

Since 130 time steps correspond to the number of years between 1880 and 2010 and 20 time steps correspond to the number of years often used in in- depth studies, we estimate the distribution of cycle times for 21 and 130 s time steps long series by running Monte Carlo simulations 100 times. The calculations for the first set were made in a matrix with 130 rows and 25 columns, A to Y.

Calculation algorithm. Column A contains a time line. Columns B and C contain the uniform random numbers. Column D and E contain the random numbers normalized to unit standard deviation. Column F contains the calculation of angles, θ, according to Eq. 1, (time window n = 3). In column G, we calculate the cycle times according to Eq. 3. (Time window n = 9 or n = 13). In column H and I we calculate the sign of the angles θ, and in Column J we calculate running LL- strength according to Eq. 2 (time windows 9 and 13). In columns K to O we calculate cycle times for 5 increasingly stronger requirements to LL-strength, x > 5/9, x > 6/9, etc. In columns P to T we calculate the number of significant cycle times. Finally, in columns U to Y, we calculate cycle amplitude for selected time windows (time windows 2, 3.. 30 years).

For 100 such calculations, we made histograms for the main results and then calculated: i) the average and the median cycle time, CT, for all points where rotations in the phase plot were consistently either positive or negative for x = 7 to 13 time steps out of 13, (and x = 5 to 9 time steps out of 9). That is, we get 5 and 7 distributions of cycle times. Since cycle time calculations contain the term n/θ, and θ can have very small values that give rise to very long cycle times, we truncated the series for CT ≈> $CT_{average}$ + 3 standard deviations.

To compare simulation results to the result from the power spectral analysis of the oceanic time series, we made a 40 steps long series with the value “1” for the numbers corresponding to cycle times found with the simulations, and the remaining steps set to “0”. All calculations are available from the authors.

4. RESULTS

Power spectral analysis. Time series for the SOI and the PDO are in Figure 2a and b. We show both the raw series and the series smoothed with the LOESS algorithm using the parameters f = 0.2 for time window and p = 2 for polynomial fitting, SigmaPlot©. Both power spectra for SOI and PDO show cycle times of 3-4 years, 7 years, 13-15 years, 22-24 years and 29-30 years, Figure 2c and d. Cycle time calculations for time series based on paired random distributions. In test runs with sampled, perfect sine functions, the design cycle times were recovered with the LL-method (Seip and Grøn 2015). For the 100 runs, LL-strengths were distributed as the histograms in Figure 3a. We have compared the distribution to a normal distribution adding the bell shaped curve in the figure. As an example, Figure 3b shows the distribution of cycles with the restriction that cycle times are only sampled if more than 8 (upper panel) and more than 9 (lower panel) of 13 time steps show LL – relations with the same sign. (In the actual calculations, we used LL – strength). The distribution is skewed towards long cycle times. (Skewness 1.4 and 0.8 respectively). For the two 21 sample length series with uniform and pseudo normal distributions respectively, we obtained 2 × 5 cycle times corresponding to the requirement that more than 5, 6, 7, 8 and 9 time steps rotate in the same direction. For the 130 sample set series, we similarly got 2 × 7 cycle times. All cycle times, except the two shortest cycle times, were significantly different at the $p < 0.05$ level for both the 21 and the 130 time steps long samples cases, and for both the uniform and the pseudo random distributions.

1

a))

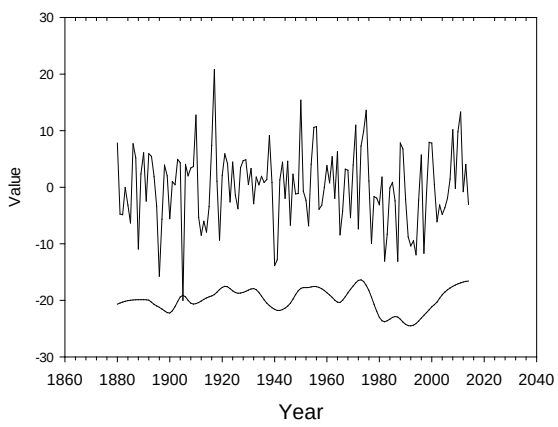
The Southern oscillation index, SOI
Upper line: raw; lower line LOESS smoothed
Value
Year

b)

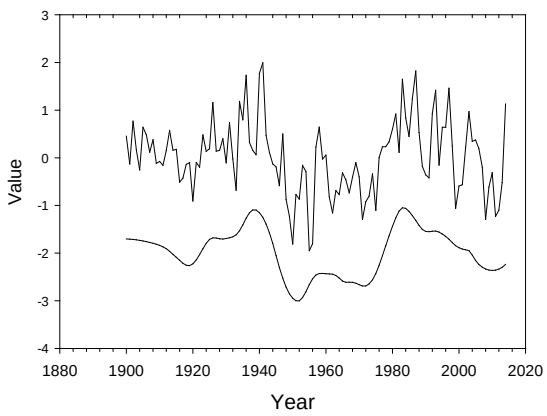
Pacific decadal oscillation, PDO
Upper line: raw; lower line LOESS smoothed
Value
Year

c)

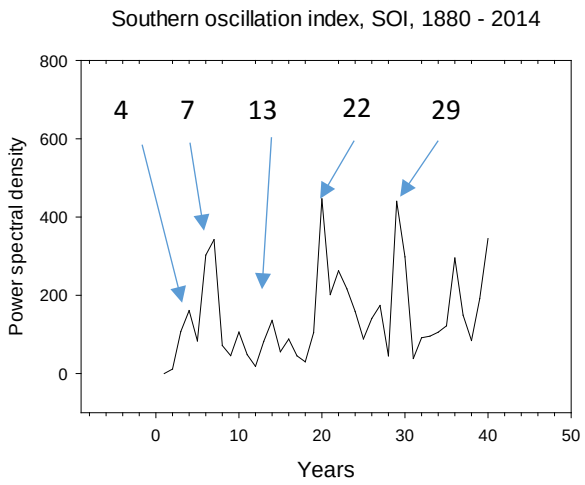
Southern oscillation index, SOI, 1880 - 2014
4
7
13
22
29
Power spectral density
Years

d)

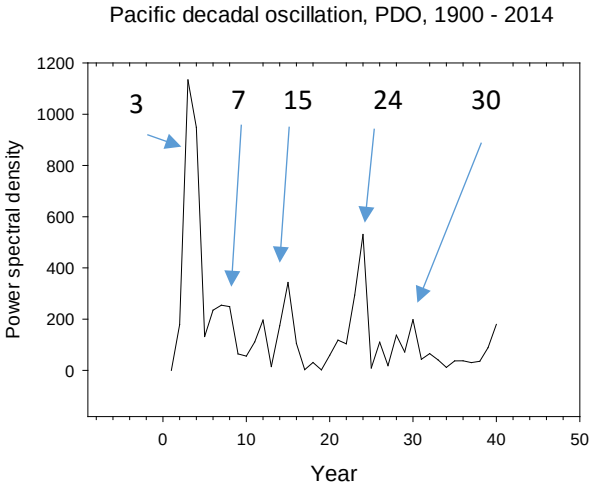
Pacific decadal oscillation, PDO, 1900 - 2014
3
7
15
24
30
Power spectral density
Year

e)

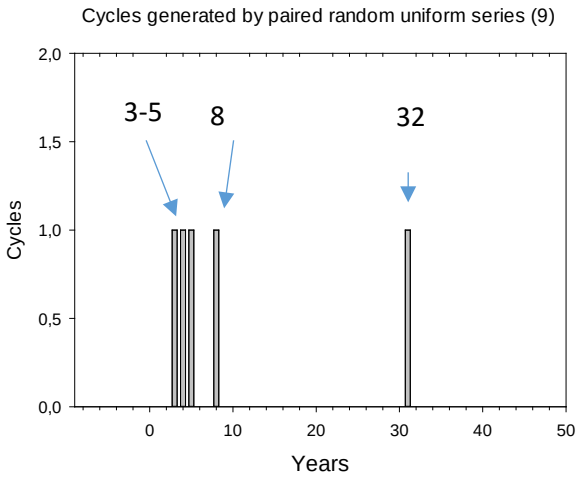
Cycles generated by paired random uniform series (9)
3-5
8
32
Cycles
Years

f)

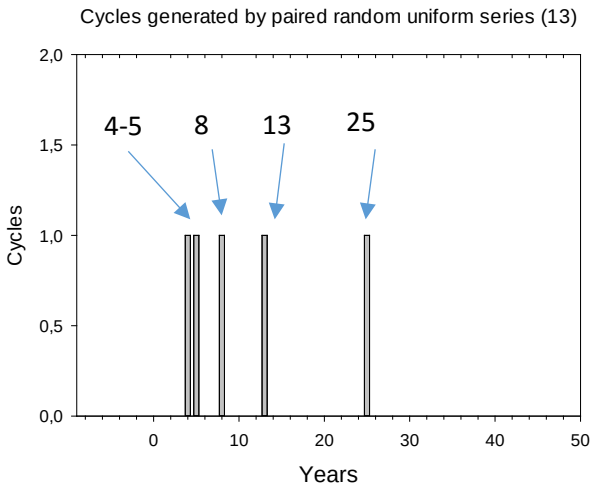
Cycles generated by paired random uniform series (13)
4-5
8
13
25
Cycles
Years

Figure 2 Cycle times. a) Time series for the Southern oscillation index. Lower line shows LOESS smoothed values with f= 0.2 and p =2 (See text); b) Time series for the Pacific decadal oscillation, PDO. Lower line shows LOESS smoothed values with f = 0.2 and p =2. c) Power spectral densities for the Southern oscillation index, SOI. d) Power spectral densities for the Pacific decadal oscillation, PDO. Numbers shows years with high power spectral density. e) Cycles generated by paired, uniform distributions with increasingly persistent leading or lagging, LL- relationships for 9 consecutive years. f) Cycles generated by paired, uniform distributions with increasingly persistent leading or lagging, LL- relations for 13 consecutive years

The distribution of cycle times with increasing requirements to persistent rotations, that is, increasing persistence of leading or lagging relations, is shown in Supplementary material 2 Figure S2 a to j.

The simulated cycle times correspond well with the cycle times in the SOI and PDO series, Figure 2. Since both sets of cycle times are associated with a fair degree of uncertainties, we estimated the probability, p, that the simulated cycle times in Figure 2e and f should correspond with the cycle times ± 1 identified in Figure 2b and c by multiplying probabilities for a fit to observed cycle times. We found $p < 0.02$.

The relationship between LL- strength, cycle time and the frequency of a given LL-strength among the 100 trials are shown in Figure 4. It is seen that the cycle time decreases with increasing LL- strength. In Figure 4a, shows that the frequency of long cycles about 40 to about 7 years forms a plateau (shaded area) and that shorter cycles are less frequent. In Figure 5b, the decreasing frequency is smooth. We also found that with paired stochastic series, cycles shorter than about 20 years show, on the average, smaller amplitudes, A, than longer cycles, reaching about half the maximum value around 7 years: $A = 0{,}83 \times \ln(CT) + 0{,}21$, $R^2 = 0.95$, $p < 0.05$

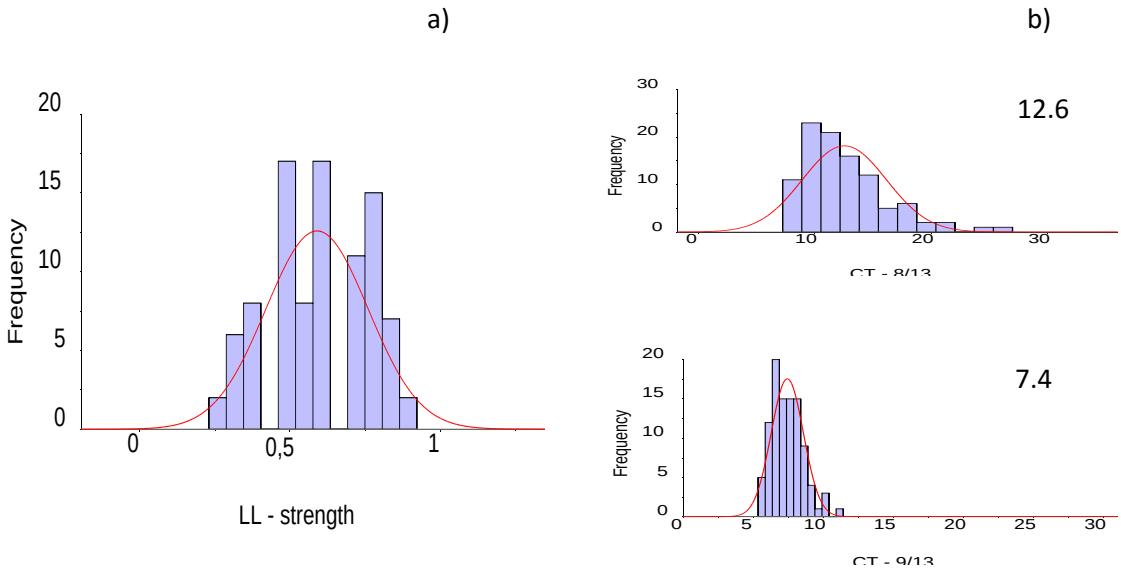

Figure 3. Histogram for Leading – lagging, LL- strength and cycle times. a) LL- strength as (N_{pos} – N_{neg}) / (N_{pos} + N_{neg}). b) Histograms for cycle times. Upper panel: 8 of 13 time steps show that one series is leading the other, cycle time is 12. 6 time steps (years) Lower panel: 9 of 13 time steps shows that one series is leading the other, cycle time is 7.4 time steps (years). Wilcoxon signed rank test shows that the two distributions are significantly different ($p < 0.001$).

5. DISCUSSION

We first discuss the similarity between our cycle times found for paired stochastic time series and cycle times found in time series for ocean currents (represented by their proxy indexes.) Thereafter, we discuss implications for potential mechanisms that may cause particular cycles in the ocean currents.

5.1 Cycle time comparisons.

Our results show similarities between dominating cycle times for paired stochastic series with leading – lagging relations and dominating cycles in PDO and SOI time series. The cycle time results for PDO and SOI are consistent with time steps reported in the literature, e.g., 4 to 6 years for El Niño southern oscillation, ENSO, reported by Tourre et al. (2001), Newman et al. (2011) and Gehne et al. (2014); and the 14 years cycle time for the interdecadal pacific oscillation, IPO, reported by Meehl et al. (2014). Wunsch (1999) find for the SOI spectral density that there is a broad peak near 4 years that is statistically significant and is an indicator of ENSO, but that below the ENSP peak, the spectral density is indistinguishable from white noise. However, he also emphasizes that this indistinction is not a proof that there might not be signals in the specter. We have found three arguments that support the SOI density spectrum as expressing real climate processes. i) The SOI and the PDO spectra show similarities in peak positions, in spite of representing different regions and being obtained by different measures. ii) Both SOI, PDO and the spectra for the random paired series have peaks around 4

years, iii) Manipulating uniformly random distributions reveals “canonical” numbers, like 4 and 5, both in leading relations between time series and in card shuffling experiments, Mann (1994), Bayer and Diaconis (1992). See Supplementary material 1. The present study suggests that forcing paired stochastic series by imposing leading lagging relations on them may also give rise to other “canonical” numbers. An approach for examining if cycles are real would be to apply a similarity measure, e.g., PCA, to several power spectra density, PSD, curves that originate from different, but related systems. An obstacle to such comparisons would be that peaks will often not be sharp, and that they can be displaced some small distances relative to each other. However, sharp spectral lines may be artifacts of the method caused by aliasing, Wunsch (2000). An alternative method is to calculate running average cycle times by the methods used by Kestin et al. (1998).

.

a) b)

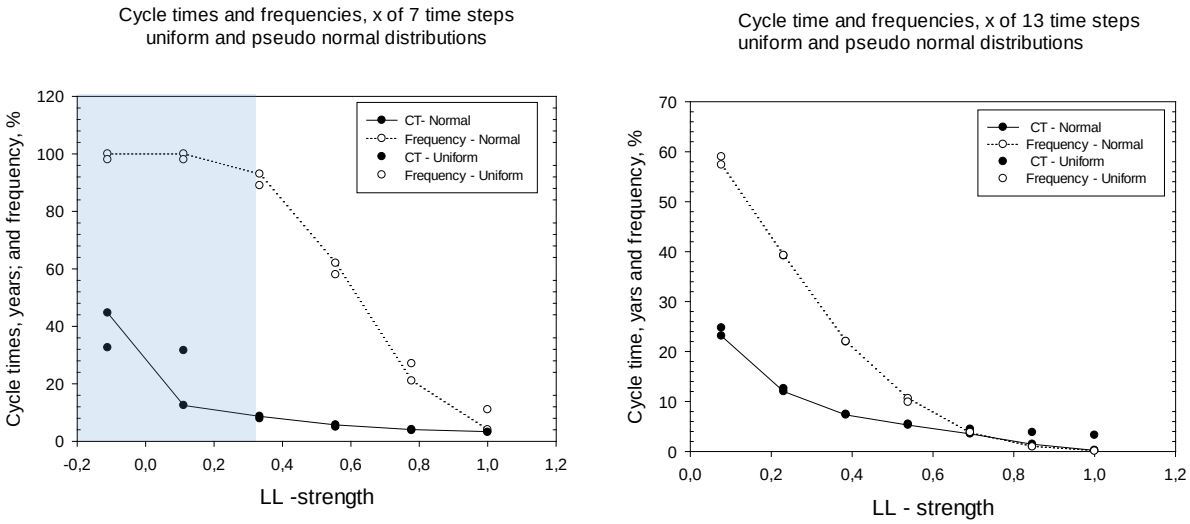

Figure 4. Cycle time and number of trials out of 100 as a function of leading- lagging, LL-strength. a) One of the random uniform time series leads the other for 5 to 9 out of 9 consecutive time steps. LL- strength of 0.5 corresponds to 7 out of 9. Shaded area shows a plateau in frequency. b) One of the time series leads the other in 7 to 13 time steps out of 13 consecutive time steps. Uniform and pseudo normal distributions gave similar results.

5.2 Possible causal mechanisms

To explain decadal and multidecadal cycles in ocean currents based on the present study, three factors are required: i) two distinguishable systems that show stochastic components, ii) one of them has to lead the other with a distinguishable lead time and iii) endogenous or internal

forces that cause one system to impact the other. It could be “bridges” between ocean currents or between the ocean or atmospheric movements.

To add context to the simulation results four issues need to be addressed: i) The meaning of time steps. ii) Forces that correspond to random impacts on the ocean - atmosphere system. iii) Forces that cause leading – lagging relations to become stronger and more frequent compared to two independent random distributions, and probably, iv) some mechanism that amplifies the cycle times induced by randomness and LL – strength.

The time steps and random forcings. The time steps in the random series must have a counterpart in the real world that the observation series are drawn from. During particular seasons of a year there appear to be events (like the south Asian Monsoon (Liu et al. 2015) that have a strong impact on the ocean- atmosphere system. Furthermore, the warm phases of ENSO tend to be strongly phase locked to the winter period of the annual cycle, (Flugel and Chang 1999). The time steps in our simulations may therefore reasonably correspond to one year.

Leading – lagging relations. We have shown that with random forcings, there is a certain probability that there will be persistent leading – lagging relations for several years. For example, there were persistent leading lagging relationships for 13 out of 13 time steps in 6 % of the trial runs. Cycle times decrease with increasing strength of the coupling between the movements in the two variables (in the present study the strength of the coupling is stochastically determined, but we have selected paired subsamples of the series with the same coupling strength.) If short cycle times < 5 years are the rule rather than the exception, there has to be forces that that make one series leading to the other more frequent than by randomness. Several studies report leading or lagging relations between oceanic oscillation variables. For example, Chylek et al. (2014 a) report that the Atlantic Multidecadal oscillation leads PDO with 12 years and Di Lorenzo et al. (2015) hypothesizes that the decadal variability of the ENSO arises from the combined action of ENSO and the Pacific meridional mode involving stochastic excitation, signal decays and time lags. Fedorov et al. (2015), their Figure 11b shows in a graph like our Figure 1b that sea surface temperature in the Nino 3 region leads a warm pool eastern edge in the Pacific with Leading-strength -0.78 and phase shift of 1.6 months (our interpretation and calculations). Capotondi et al. (2015) summarize results on teleconnections and their impacts. However, they also suggest that the physical processes responsible for the connection are not yet (2016) understood.

Cycle amplitude. As a backdrop for examining the relation between cycle time and cycle amplitude, we examined the effect of finding higher amplitude by extending the sampling interval and thereby increasing the probability of finding higher and lower time series values in the stochastic series. We found that large amplitudes were prevalent above cycle times of about 20 samples (years) consistent with McPhaden (2015) quoting 15 – 20 years as the occurrence rate of

extreme El Niños. The amplitude for 7 year cycles are about half of the maximum amplitude. A factor 2:1 also seems to be characteristic for strong and moderate ENSO events, Takahashi and Dewitte (2016). However, there may be factors that are associated with extreme events and that make the amplitude relatively stronger than by mere stochastic movements.

Amplifying forces. Although our simulations gave clear signals for most cycle times there might also be amplifying mechanisms that determine the cycle times induced by randomness and LL-strength.

We have chosen running average time windows of 9 and 13 steps to examine leading – lagging relationships. Other time windows could also have been chosen. We used uniform and pseudo normal random distributions, but non-random distributions should also be examined. A third choice would have been to subsample events that have a fixed LL –strength of say 8 out of 13 samples (years). However, with the choices we made, cycle times correspond well with those observed, supporting the results as robust.

Biological responses to abiotic factors may change with global warming, both because of increased average warming, but also because of changes in the intensity and frequency of cold and warm temperature regimes (Moore et al. 2008). Thus, the ability to predict the direction and strength of ocean currents is important in a management perspective.

Our statistical results on interaction strength and cycle times should be linked to the physical mechanisms that mediate them. To our knowledge, there are no systematic quantifications of interaction strengths and cycle times available. However, we believe that our LL-strength method would allow investigations that could identify and quantify them:. i) By testing the strength of the "bridges" in terms of LL- strength, we hypothesize that it will be possible to predict cycle times for ocean currents. ii) If there are, say, three movements that interact, it should be possible to distinguish the two pairs of interactions, and relate them to cycle times in the target variable. iii) It should be possible to test the conjecture that increased global warming, in terms of increased average SST, will cause more frequent shifts between warm and cold periods by examining leading - lagging relations between candidate ocean currents, or between ocean currents and the atmosphere, c.f., summary in Santoso et al. (2015). Importantly, the test can be applied to both observed data and to data generated by model simulations, e.g. as in Cai et al. (2015) and Fedorov et al. (2015) or to physical experiments.

Our results on distinct cycle times are based on simulations. There may be a statistical intuition that would explain, or make clear, why cycle times becomes distinct. However, we have not managed to work out such an intuition.

6. Conclusion

Our study suggests that cycle time in ocean currents, expressed by their proxies: e.g., the "Pacific decadal oscillation", PDO, and

the “Southern oscillation index”, SOI, are determined by the degree to which one current is able to modulate the other current. The leading, current may have stochastic characteristics. Our results show that stronger LL- relations for the two currents give shorter common cycle times. There may be superimposed several cycle with different cycle times in the time series. For the three time series studied here, the PDO, the SOI and the synthetic set of paired stochastic time series, we get distinct cycle times of 2-5, 7-8, 13-15, 22-24, and 29-30 years. The short cycles, 2 to 5 years, correspond to a significant broad peak in the SOI index identified by Wunsch (1999). Longer cycle times can not be identified significantly in the SOI, but since they can be identified both in SOI and PDO, our belief that the cycles reflect real movements in the ocean currents is strengthened. Lastly, finding distinct cycles in ocean currents that do not involve other exogenous factors than mechanisms that cause leading lagging relations may be somewhat surprising. However, it may extend a similar “somewhat surprising” finding reported by Mann (1994), p.1, that there is a “canonical” number for shuffling card decks. Both processes involve manipulation of uniformely random distributions.

Acknowledgement

We thank the University college of Oslo and Akershus for applied sciences for supporting our study and Shineng Hu for supplying us with data for Figure 11b in Fedorov et al. (2015).

Author contribution

KLS devised the original idea for the method and wrote the paper. Ø.G. supplied additional mathematical foundation for method and co-wrote the manuscript.

There is no competing financial interests for any of the authors

Correspondence and request for materials should be addressed to knut.lehre.seip@hioa.no.

References

Allan, R. J. and R. D. D'Arrigo (1999). "'Persistent' ENSO sequences: how unusual was the 1990-1995 El Nino?" Holocene **9**(1): 101-118.

Amaya, D. J., S. P. Xie, A. J. Miller and M. J. McPhaden (2015). "Seasonality of tropical Pacific decadal trends associated with the 21st century global warming hiatus." Journal of Geophysical Research-Oceans **120**(10): 6782-6798.

Andrews, M. B., J. R. Knight and L. J. Gray (2015). "A simulated lagged response of the North Atlantic Oscillation to the solar cycle over the period 1960-2009." Environmental Research Letters **10**(5).

Bayer, D. and P. Diaconis (1992). "Trailing the dovetail shuffle to its lair." Ann. appl. probab. **2**(2): 294-313.

Cai, W. J., G. J. Wang, A. Santoso, M. J. McPhaden, L. X. Wu, F. F. Jin, A. Timmermann, M. Collins, G. Vecchi, M. Lengaigne, M. H. England, D. Dommenget, K. Takahashi and E. Guilyardi (2015). "Increased frequency of extreme La Nina events under greenhouse warming." Nature Climate Change **5**(2): 132-137.

Capotondi, A., A. T. Wittenberg, M. Newman, E. Di Lorenzo, J. Y. Yu, P. Braconnot, J. Cole, B. Dewitte, B. Giese, E. Guilyardi, F. F. Jin, K. Karnauskas, B. Kirtman, T. Lee, N. Schneider, Y. Xue and S. W. Yeh (2015). "Understanding ENSO Diversity." Bulletin of the American Meteorological Society **96**(6): 921-938.

Chylek, P., M. K. Dubey, G. Lesins, J. N. Li and N. Hengartner (2014 a). "Imprint of the Atlantic multi-decadal oscillation and Pacific decadal oscillation on southwestern US climate: past, present, and future." Climate Dynamics **43**(1-2): 119-129.

DelSole, T., M. K. Tippett and J. Shukla (2011). "A Significant Component of Unforced Multidecadal Variability in the Recent Acceleration of Global Warming." Journal of Climate **24**(3): 909-926.

Di Lorenzo, E., G. Liguori, N. Schneider, J. C. Furtado, B. T. Anderson and M. A. Alexander (2015). "ENSO and meridional modes: A null hypothesis for Pacific climate variability." Geophysical Research Letters **42**(21): 9440-9448.

Fedorov, A. V., S. N. Hu, M. Lengaigne and E. Guilyardi (2015). "The impact of westerly wind bursts and ocean initial state on the development, and diversity of El Nino events." Climate Dynamics **44**(5-6): 1381-1401.

Finlay, K., R. J. Vogt, M. J. Bogard, B. Wissel, B. M. Tutolo, G. L. Simpson and P. R. Leavitt (2015). "Decrease in CO_2 efflux from northern hardwater lakes with increasing atmospheric warming." Nature **519**(7542): 215-218.

Flugel, M. and P. Chang (1999). "Stochastically induced climate shift of El Nino-Southern Oscillation." Geophysical Research Letters **26**(16): 2473-2476.

Gehne, M., R. Kleeman and K. E. Trenberth (2014). "Irregularity and decadal variation in ENSO: a simplified model based on Principal Oscillatory Petterns." Clim Dyn.

Keeling, C. D. and T. P. Whorf (1997). "Possible forcing of global temperature by oceanic tides." Proc. Natl. Acad. Sci. USA **94**: 8321-8328.

Kestin, T. S., D. J. Karoly, J. I. Yang and N. A. Rayner (1998). "Time-frequency variability of ENSO and stochastic simulations." Journal of Climate **11**(9): 2258-2272.

Liu, B. Q., G. X. Wu and R. C. Ren (2015). "Influences of ENSO on the vertical coupling of atmospheric circulation during the onset of South Asian summer monsoon." Climate Dynamics **45**(7-8): 1859-1875.

Mann, B. (1994). "How many times should you shuffle a deck of cards?" UMAP J. **4**: 303-332.

McCarthy, G. D., I. D. Haigh, J. J. M. Hirschi, J. P. Grist and D. A. Smeed (2015). "Ocean impact on decadal Atlantic climate variability revealed by sea-level observations." Nature **521**(7553): 508-U172.

McPhaden, M. J. (2015). "COMMENTARY: Playing hide and seek with El Nino." Nature Climate Change **5**(9): 791-795.

Meehl, G. A., J. M. Arblaster, K. Matthes, F. Sassi and H. van Loon (2009). "Amplifying the Pacific Climate System Response to a Small 11-Year Solar Cycle Forcing." Science **325**(5944): 1114-1118.

Meehl, G. A., A. X. Hu, J. M. Arblaster, J. Fasullo and K. E. Trenberth (2013). "Externally Forced and Internally Generated Decadal Climate Variability Associated with the Interdecadal Pacific Oscillation." Journal of Climate **26**(18): 7298-7310.

Meehl, G. A., H. Y. Teng and J. M. Arblaster (2014). "Climate model simulations of the observed early-2000s hiatus of global warming." Nature Climate Change **4**(10): 898-902.

Moore, S. K., N. J. Mantua, J. P. Kellogg and J. A. Newton (2008). "Local and large-scale climate forcing of Puget Sound oceanographic properties on seasonal to interdecadal timescales." Limnology and Oceanography **53**(5): 1746-1758.

Munk, W., M. Dzieciuch and S. Jayne (2002). "Millennial climate variability: Is there a tidal connection?" Journal of Climate **15**(4): 370-385.

Newman, M., S. I. Shin and M. A. Alexander (2011). "Natural variation in ENSO flavors." Geophysical Research Letters **38**.

Press, W. H., B. P. Flannery, S. A. Teukolsky and W. T. Vettering (1986). Numerical recipes. The art of scientific computing. Cambridge, Cambridge university press.

Ray, R. D. (2007). "Decadal climate variability: Is there a tidal connection?" Journal of Climate **20**(14): 3542-3560.

Santoso, A., W. J. Cai, M. Collins, M. McPhaden, F. F. Jin, E. Guilyardi, G. Vecchi, D. Dommenget and G. J. Wang (2015). "ENSO extremes and diversity. Dynamics, Teleconnections, and Impacts." Bulletin of the American Meteorological Society **96**(11): 1969-1972.

Seip, K. L. (2015). "Investigating possible causal relations among physical, chemical and biological variables across regions in the Gulf of Maine." Hydrobiologia **744**: 127-143.

Seip, K. L. and Ø. Grøn (2015). "A new method for identifying possible causal relationships between CO_2, total solar irradiance and global temperature change." Theoretical and Applied Climatology **In print**.

Seip, K. L., H. Sas and S. Vermij (1990). "The short term response to eutrophication abatement." Aquatic Sciences **52**: 199-220.

Takahashi, K. and B. Dewitte (2016). "Strong and moderate nonlinear El Nino regimes." Climate Dynamics **46**(5-6): 1627-1645.

Timmermann, A., J. Oberhuber, A. Bacher, M. Esch, M. Latif and E. Roeckner (1999). "Increased El Nino frequency in a climate model forced by future greenhouse warming." Nature **398**(6729): 694-697.

Tourre, Y. M., B. Rajagopalan, Y. Kushnir, M. Barlow and W. B. White (2001). "Patterns of coherent decadal and interdecadal climate signals in the Pacific Basin during the 20th century." Geophysical Research Letters **28**(10): 2069-2072.

Trenberth, K. E. (2015). "Has there been a hiatus?" Science **349**(6249): 691-692.

Wunsch, C. (1999). "The interpretation of short climate records, with comments on the North Atlantic and Southern Oscillations." Bulletin of the American Meteorological Society **80**(2): 245-255.

Wunsch, C. (2000). "On sharp spectral lines in the climate record and the millennial peak." Paleoceanography **15**(4): 417-424.

Zhu, J., G. Zhou, R. H. Zhang and Z. Sun (2011). "On the role of oceanic entrainment temperature (T-e) in decadal changes of El Nino/Southern Oscillation." Annales Geophysicae **29**(3): 529-540.